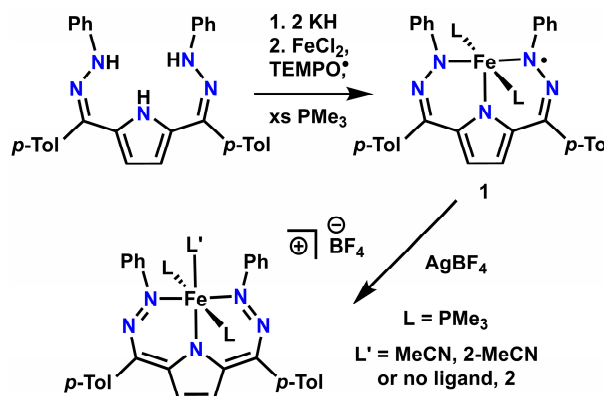# Iron(II) Complexes Featuring a Redox-Active Dihydrazonopyrrole Ligand

Kate A. Jesse,[a] Mu-Chieh Chang,[b] Alexander S. Filatov,[a] and John S. Anderson*[a]

Abstract: Nature uses control of the secondary coordination sphere to facilitate an astounding variety of transformations. Similarly, synthetic chemists have found metal-ligand cooperativity to be a powerful strategy for designing complexes that can mediate challenging reactivity. In particular, this strategy has been used to facilitate two electron reactions with first row transition metals that more typically engage in one electron redox processes. While NNN pincer ligands feature prominently in this area, examples which can potentially engage in both proton and electron transfer are less common. Dihydrazonopyrrole (DHP) ligands have been isolated in a variety of redox and protonation states when complexed to Ni. However, the redox-state of this ligand scaffold is less obvious when complexed to metal centers with more accessible redox couples. Here, we synthesize a new series of Fe-DHP complexes in two distinct oxidation states. Detailed characterization supports that the redox-chemistry in this set is still primarily ligand based. Finally, these complexes exist as 5-coordinate species with an open coordination site offering the possibility of enhanced reactivity.

Scheme 1. Synthesis of **1** and **2**.

Coordinated movement of electron and proton transfer during catalysis is vital for productive reactivity in challenging chemical transformations. Second and third row transition metals facilitate an astounding variety of reactions due to their ability to engage in multi-electron and multi-proton elementary steps (i.e. oxidative addition of hydrogen).[1] However, these metals are often expensive and toxic, providing motivation for the development of catalysts featuring metals such as Fe, which is cheap, largely nontoxic, and widely available. In nature, elegant secondary coordination spheres in enzymatic active sites feature redox-active cofactors, hydrogen-bonding networks, and proton shuttling pathways which enable difficult transformations with first-row metals.[2] Using these natural systems as inspiration, many synthetic chemists have worked to develop supporting ligands that can similarly shuttle protons or electrons to substrates.[3,4] Pincer ligands with an NNN binding pocket feature prominently in this area, particularly as redox non innocent supporting scaffolds.[5] However, pincer scaffolds which can support both proton *and* electron transfer are comparatively rarer.[6]

Our laboratory has been exploring this area through the use of dihydrazonopyrrole (DHP) ligand scaffolds. We have found that Ni complexes of this family do demonstrate reversible ligand-based storage of both protons and electrons as well as engaging in oxidative small molecule reactivity.[7] The redox-activity of this system is predominantly ligand based as Ni centers, particularly in square planar geometries, have a strong bias for a divalent

oxidation state. As such, we were interested in exploring complexes where the localization of redox reactions was more ambiguous due to a more redox metal center, namely Fe, which readily populates both Fe(II) and Fe(III) oxidation states. Here we report the development of Fe complexes of the ligand ^{Ph,Tol}DHP (2,5-bis((2-phenylhydrazono)(p-tolyl)methyl)-pyrrole) in two distinct oxidation states. These complexes adopt 5- or 6-coordinate geometries which opens up additional possible sites for substrate binding and reactivity. Unlike the related Ni-system, we have been unable to isolate ligand-hydrogenated complexes with Fe, however, the initial metalation reaction requires the presence of an external H-atom abstractor, suggesting that ligand-based H-atoms are present as reactive intermediates. Most importantly, we have performed detailed characterization of the electronic structure of these complexes revealing that despite the enhanced redox-flexibility of the Fe center, oxidation is still predominantly localized on the supporting pincer ligand. This suggests that Fe complexes could exhibit enhanced reactivity due to the possibility of combined ligand- and metal-based redox reactivity.

The previously reported ^{Ph,Tol}DHP ligand[7c] was deprotonated with two equivalents of KH in THF, then filtered and condensed to form a red powder putatively assigned as the doubly deprotonated ligand salt. This powder was added dropwise as a suspension to a 1:1 mixture of FeCl$_2$ and TEMPO$^•$ in diethylether in the presence of excess PMe$_3$. After work-up, (^{Ph,Tol}DHP$^•$)Fe(PMe$_3$)$_2$ (**1**) is obtained as a dark green solid in 31% crystalline yield (Scheme 1). IR spectroscopy shows no evidence for the presence of any N–H features suggesting that the additional H-atoms present on ^{Ph,Tol}DHP have been abstracted as H-atoms by the added TEMPO$^•$. While we do not have evidence for any Fe-containing species with N–H functionalities, we note that syntheses carried out in the absence of TEMPO$^•$ result in a red-brown solid that appears to be a complex mixture of products by NMR spectroscopy. The need for an H-atom abstractor to form **1** suggests that such hydrogenated ligand complexes are likely intermediates, as has been observed in the related Ni systems.[7c]

Single crystals of **1** suitable for single-crystal X-ray diffraction (SXRD) were grown from a vapor diffusion of petroleum ether into toluene at room temperature overnight (Figure 1). The SXRD structure of **1** reveals an intermediate geometry between square pyramidal and trigonal bipyramidal (τ_5 = 0.45). The ^{Ph,Tol}DHP ligand is bound symmetrically through the beta-N of the hydrazone arms while the two PMe$_3$ ligands are trans to each other. The Fe-N$_{hydrazone}$ bond distance averages 1.923(2) Å while the Fe-N$_{pyrrole}$ bond distance is 1.937(2) Å (Table 1). These long

[a] University of Chicago Department of Chemistry, 929 E 57th St. Chicago, IL, 60637

[b] National Taiwan University Department of Chemistry, No. 1, Section 4, Roosevelt Rd, Da'an District, Taipei City, Taiwan 10.

Supporting information for this article is given via a link at the end of the document.((Please delete this text if not appropriate))
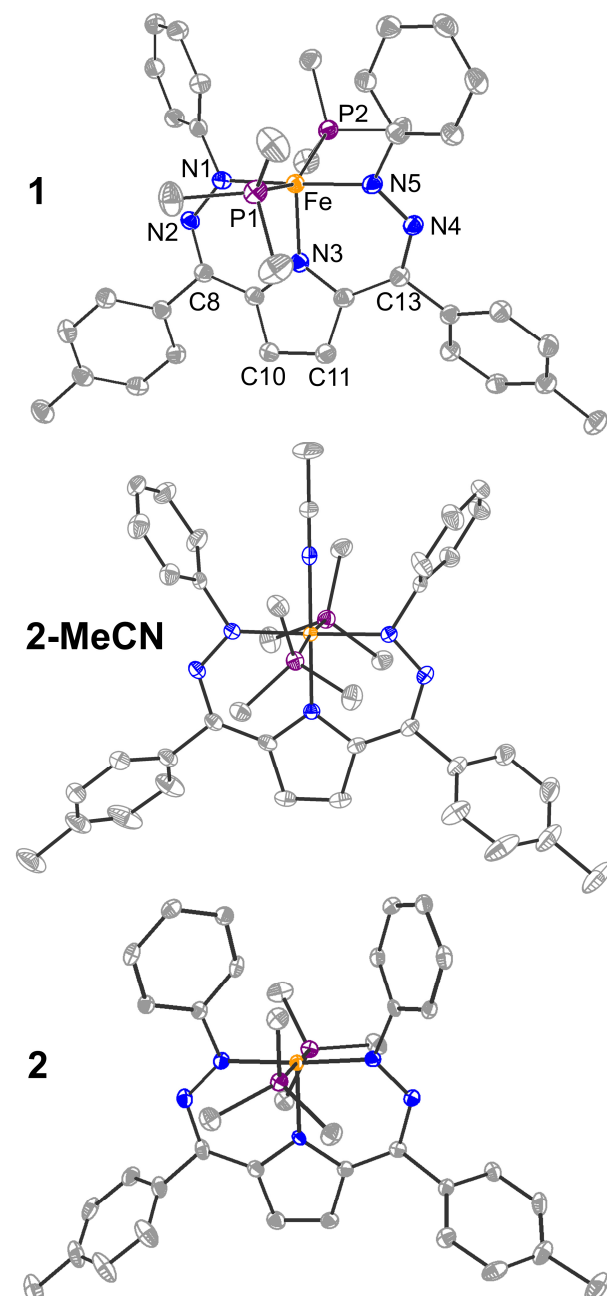
Figure 1. Solid state structures of **1**, **2-MeCN**, and **2**. Ellipsoids are set to 50% probability. Hydrogen atoms and counterions have been ommitted for clarity. Fe is shown in orange, C in grey, N in blue, and P in purple.

Fe-ligand distances are suggestive of a high spin Fe center. Consistent with this hypothesis, the ^{1}H NMR shows four broadened and shifted signals as would be expected for a paramagnetic complex (see SI). Evan's method gives a μ_{eff} of 4.6 B.M. consistent with an overall spin of $S = ^3/_2$. Similarly, EPR of **1** shows an $S = ^3/_2$ rhombic signal featuring g_{eff} values at $g =$ 5.13, 2.83, and 1.81 (see SI). This overall spin suggests that the complex is best assigned as either a high spin Fe(II) complex anti-ferromagnetically coupled to a dianinoic ^{Ph,Tol}DHP ligand-based radical (^{Ph,Tol}DHP$^{\bullet}$) or as a high spin Fe(I) center featuring an oxidized mono-anionic ligand.

Comparison to Ni complexes featuring the same ^{Ph,Tol}DHP ligand in oxidized and radical states (Table 1) indicates **1** is best considered an Fe(II) center antiferromagnetically coupled to a ligand radical. The C–C pyrrole backbone, N-N, and N-C bond

Table 1. Selected bond lengths of **1**, **2**, **2-MeCN**, and related Ni complexes (Å)

	1	2 -MeCN	2	Ni(^{Ph,Tol}DHP$^{\bullet}$)[a]	[Ni(^{Ph,Tol}DHP)]$^{+}$ [a,b]
M[c]-N1	1.930(2)	1.923(2)	1.875(2)	1.866(2)	1.864(2)
M-N3	1.937(2)	1.916(2)	1.861(2)	1.863(2)	1.860(2)
M-N5	1.916(2)	-	1.861(2)	1.872(2)	1.869(2)
M-P1	2.3980(6)	2.3343(5)	2.3657(9)	2.2319(7)	2.2630(7)
M-P2	2.4219(6)	-	2.3289(9)	-	-
N1-N2	1.351(2)	1.318(2)	1.329(3)	1.342(2)	1.302(2)
N2-C8	1.306(3)	1.345(2)	1.350(3)	1.319(3)	1.348(2)
N4-C13	1.316(3)	-	1.347(4)	1.322(2)	1.342(3)
N4-N5	1.356(3)	-	1.330(3)	1.337(3)	1.314(2)
C10-C11	1.393(3)	1.354(4)	1.351(4)	1.371(3)	1.346(3)

[a] These complexes also feature a PMe$_3$ ligand. [7c]
[b] BF$_4$ counterion
[c] M = Fe for **1**, **2-MeCN**, and **2**. M = Ni for Ni(^{Ph,Tol}DHP$^{\bullet}$) and [Ni(^{Ph,Tol}DHP)]$^{+}$

distances most closely align with a ligand radical. This assignment is supported by density functional theory (DFT) calculations. Optimization of **1** was first attempted as a quartet, but resulted in a complex with two unpaired electrons on Fe ferromagnetically coupled to a ligand based radical. This electronic configuration seemed unlikely, so **1** was then optimized with a broken symmetry treatment. This shows spin density on the ligand of opposite character from the spin density on the high-spin Fe(II) center. Mulliken spin density indicates that 0.72 electrons are localized on ^{Tol,Ph}DHP, supporting the assignment of a primarily ligand based radical (see SI).

Cyclic voltammetry of **1** in THF shows a reversible feature at −0.73 V and a quasi-reversible feature at −1.31 V vs. Fc/Fc$^+$ (see SI).These features are similar to those observed in related Ni systems suggesting that these redox events are ligand based despite the possibility of Fe-based redox chemistry.[7] Interestingly, there are not any additional redox couples that might be assigned to an Fe-based oxidation within the THF solvent window. Unfortunately, attempts to reduce **1** with a variety of reagents invariably led to a complex mixture of products. However, as might be predicted by the reversibility of the feature at −0.73 V vs. Fc/Fc$^+$, oxidation of **1** with AgBF$_4$ in acetonitrile is more tractable and addition of oxidant results in an immediate color change from deep green to dark blue. Further color changes are observed upon workup and drying, and the oxidized complex [(^{Ph,Tol}DHP)Fe(PMe$_3$)$_2$][BF$_4$] (**2**) is isolated as a maroon powder in-91% yield. Notably, this maroon solid regains a blue color if redissolved in acetonitrile. ^{1}H NMR of **2** in CD$_3$CN shows a symmetric diamagnetic species with two bound PMe$_3$ ligands (SI). This indicates that upon oxidation, the Fe(II) center transitions from a high spin manifold to a low spin manifold. While Fe(II) complexes feature prominently in spin-crossover applications,[8] examples where spin-crossover can be triggered by redox events are still uncommon.[9]

Single crystals suitable for X-ray diffraction were grown by vapor diffusion of diethylether into concentrated acetonitrile solutions. The SXRD structure obtained from crystals grown in this way shows a pseudo-octahedral geometry, with an acetonitrile adduct in the previously open coordination site trans to the pyrrole N to give the solvento adduct **2-MeCN** (Figure 1). As would be expected for a low spin Fe(II) center, the Fe-N$_{hydrazone}$ and Fe-N$_{pyrrole}$ distances show a slight contraction from those of **1** to 1.923(1) and 1.916(2) Å respectively. Additionally, the pyrrole C-C backbone bond is contracted to 1.354(4) Å, indicative of ligand oxidation (Table 1).

Given that an acetonitrile adduct was observed from the dark blue crystals analyzed by X-ray diffraction, we hypothesized that the color changes observed upon drying/dissolution may arise from acetonitrile binding. To investigate this, **2** was dried, then dissolved in a variety of solvents. It was found that in

coordinating solvents such as acetonitrile or DMF, the solution turned blue, while in less coordinating solvents, such as THF, the solution turned green. In benzene, **2** was sparingly soluble and produced a red solution (see SI). Together, these observations suggested that the color changes for **2** were arising from variable solvent coordination. To investigate the possibility of a solvent-free 5-coordinate complex, **2** was crystallized from a vapor diffusion of petroleum ether into THF. The SXRD structure obtained from these pale green crystals show a 5-coordinate pseudo-square pyramidal complex (τ_5 = 0.04). The ligand bond distances are a close match for those found in complex **2-MeCN**, consistent with an oxidized ^{Ph,Tol}DHP ligand (Table 1). Furthermore, the Fe–N and Fe–P distances are similar to **2-MeCN** suggesting that in both cases this oxidized complex features a low-spin Fe center. These combined observations suggest that **2** can bind solvents in its open coordination site, but that it maintains a low-spin Fe(II) electronic structure throughout. Therefore, the change from a high spin Fe(II) center in **1** to a low spin Fe(II) center in **2** is a product of ligand oxidation rather than solvent coordination.

All of the data acquired on **1** and **2** support ligand-based oxidation events. However, concretely assigning ligand versus metal-based redox localization is challenging and typically requires multiple orthogonal analyses. To further verify that the oxidation of **1** to **2** was ligand-based, Fe K-edge X-ray absorption spectroscopy (XAS) was conducted on solid powders of the two complexes. Overlaying the X-ray absorption near edge structure (XANES) spectra of these complexes show that **1** and **2** have effectively identical K-edge's at 7121.3 eV (Figure 2). This data concretely supports that the oxidation state of Fe in **1** and **2** is the same, and that the oxidation is ligand-based.

By UV-visible spectroscopy, **2** dissolved in acetonitrile features two additional absorbances at 644 and 940 nm as compared to the UV-visible spectrum of **2** in benzene (See SI). Interestingly, these absorbances align reasonably well with absorbances seen in **1** at 616 and 912 nm respectively. In particular, broad absorbances in the 800 to 1000 nm range have been seen in related Ni complexes that feature a DHP ligand radical.[8] The presence of these features may imply that in solution with coordinating solvents such as acetonitrile **2** might adopt an electronic structure with a low-spin Fe(III) metal center antiferromagnetically coupled to a ligand based radical. Notably, in the solid state **2-MeCN** shows no evidence for variable temperature redox-changes, as the structures collected at both 100 K and at room temperature show nearly identical parameters (see SI). To investigate the possibility of a redox tautomerization in solution, XAS was collected of **2-MeCN** in a polyethylene glycol matrix with added acetonitrile. However, the XANES spectrum for **2-MeCN** prepared in this way shows a similar edge position to that observed for **1** and **2**. These data suggest that the difference in UV-visible spectra between **2-MeCN** and **2** arises from the changing coordination environment at the Fe center as opposed to a different redox distribution induced by ligand binding.

The data presented here describe a series of Fe(II) complexes in various redox states. Notably, while Fe should possess an accessible Fe(III) oxidation state, all structural and spectroscopic characterization of the products indicate that these redox events are primarily ligand based. While the Fe oxidation state does not appear to change upon oxidation, the Fe(II) center does undergo a redox-induced spin-crossover from high-spin to low-spin. Finally, the oxidized complex **2** displays solvatochromism arising from solvent binding in the open coordination site in this complex. While hydrogenated versions of **1** and **2** have not been isolated, the need for an H-atom abstractor (TEMPO•) in the synthesis of **1** suggests that hydrogenated complexes are present as reactive intermediates. Further investigation into the hydrogenative and reductive chemistry of Fe complexes with DHP ligands is currently underway.

Experimental Section
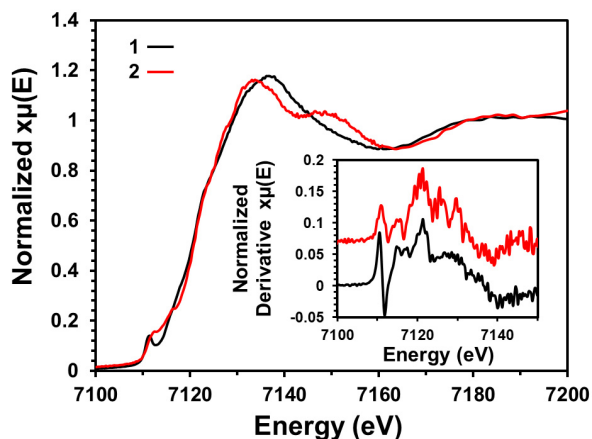
Figure 2. Fe K-edge X-ray absorption spectra of **1** and **2** as powders. Both samples feature a K-edge inflection point at 7121.3 eV. Inset: Derivative spectra of K-edge XAS. **2** is offset for ease of visualization.

General Methods

All chemicals were purchased from commercial suppliers and used without further purification. All manipulations were carried out under an atmosphere of N_2 using standard Schlenk and glovebox techniques. Glassware was dried at 180 °C for a minimum of two hours and cooled under vacuum prior to use. Solvents were dried on a solvent purification system from Pure Process Technologies and stored over 4 Å molecular sieves under N_2. Tetrahydrofuran (THF) and diethyl ether (Et_2O) was stirred over NaK alloy and run through an additional alumina column prior to use to ensure dryness. Solvents were tested for H_2O and O_2 using a standard solution of sodium-benzophenone ketyl radical anion. CD_3CN, C_6D_6, and d_8-toluene were dried over 4 Å molecular sieves under N_2. ^1H, $^{13}C\{^1H\}$, $^{31}P\{^1H\}$, $^{19}F\{^1H\}$, and $^{11}B\{^1H\}$ NMR spectra were recorded on Bruker DRX 400 or 500 spectrometers. Chemical shifts are reported in ppm units referenced to residual solvent resonances for ^1H and $^{13}C\{^1H\}$ spectra. UV-visible spectra were recorded on a Bruker Evolution 300 spectrometer and analyzed using VisionPro softwar. IR spectra were obtained on a Bruker Tensor II spectrometer with the OPUS software suite. All IR samples were prepared nujol mulls and collected between KBr plates. EPR spectra were recorded on an Elexsys E500 Spectrometer with an Oxford ESR 900 X-band cryostat and a Bruker Cold-Edge Stinger. EPR data was fit using a least-squares fit in SpinCount. Electrochemical measurements were performed using a BAS Epsilon potentiostat and analyzed using BAS Epsilon software version 1.40.67NT. Cyclic voltammetry measurements were made using a glassy carbon working electrode, platinum wire counter electrode, and silver wire pseudo-reference electrode, and referenced to external Fc/Fc+. Single crystal X-ray diffraction data were collected in-house using Bruker D8 Venture diffractometer equipped with Mo microfocus X-ray tube (λ = 0.71073 Å) or at the Advanced Photon Source of Argonne National Laboratory (beamline 15-ID-B,C,D) using X-ray radiation with a wavelength of λ = 0.41328 Å. X-ray near-edge absorption spectra (XANES) were employed to probe the local environment of Fe. Powder samples were prepared by material grinding finely. A Teflon window was sealed on one side with Kapton tape and powder was then transfer transferred to the inside of this ring before compacting with a Teflon rod and sealing the remaining face with Kapton tape. In the case of RT solution samples, powder was dissolved with minimal solvent, then added to melted polyethylene glycol and mixed well. This was allowed to cool then transfered to a teflon window sealed on one side with Kapton tape. After transfer of the material, the window was sealed with Kapton tape. All sample preparation was performed under an inert atmosphere. Data were acquired at the Advanced Photon Source at Argonne National Labs with a bending magnet source with ring energy at 7.00 GeV. Fe K-edge data were acquired at the MRCAT

MRCAT 9-BM-B,C and 10-BM beam lines. The incident, transmitted and reference X-ray intensities were monitored using gas ionization chambers. A metallic iron foil standard was used as a reference for energy calibration and was measured simultaneously with experimental samples. X-ray absorption spectra were collected at room temperature. Data collected was processed using the Demeter software suite[10] by extracting the EXAFS oscillations $\chi(k)$ as a function of photoelectron wavenumber k. The theoretical paths were generated using FEFF6 and the models were determined using the fitting program Artemis.

Syntheses

Fe(PhDHP*)(PMe$_3$)$_2$ (1)

In a 20 mL vial, PhDHP-H$_2$ (500 mg, 1 eq.) was dissolved in THF (10 mL) with stirring. KH (83 mg, 2 equiv.) were added as a solid and allowed react until all bubbling had stopped (~10 minutes) and the solution was bright red. The solution was then filtered and condensed under vacuum to form a red oil. This was taken up in petroleum ether and then dried under vacuum to form a red powder (PhDHP-K$_2$). In a 20 mL vial, FeCl$_2$ (11.3 mg, 0.09 mmol, 1 eq.) was dissolved in diethyl ether (12 mL) in the presence of excess PMe$_3$ (0.1 mL, 0.9 mmol, 10 eq.) and TEMPO• (15.3 mg, 0.1 mmol, 1.1 eq.) to form a deep read solution. Separately, PhDHP-K$_2$ (50 mg, 0.09 mmol, 1 equiv.) was stirred in diethyl ether (5 mL) to form a suspension. This suspension was added dropwise to form a deep green solution. Once the PhDHP-K$_2$ had been added, the reaction was allowed to stir for 20 minutes, filtered, then condensed under vacuum. This was washed with petroleum ether (10 mL), taken up in toluene again (4 mL), filtered, and dried under vacuum. This was taken up in toluene (4 mL), filtered, then condensed to a concentrated solution. The pure product was obtained by a two-layer crystallization of petroleum ether and the concentrated reaction solution in toluene at −35 °C. Yield: 31%. Single crystals suitable for XRD were obtained by a vapor diffusion of petroleum ether into a concentrated solution of product in toluene at room temperature overnight. ^{1}H NMR (400 MHz, d_8-toluene , RT): δ = 25.49 (bs), 15.00 (bs), 13.13 (bs), −5.80 (bs). Magnetic Susceptibility: Evans' Method (C$_6$D$_6$, RT, μ$_B$): μ$_{eff}$ = 4.6. EPR experimental (g$_{eff}$): 5.13, 2.83, 1.81. EPR simulated (g$_z$, g$_x$, g$_y$): 2.17, 2.28, 1.98. IR (nujol mull, cm^{-1}): 2794 (C-H, w), 1583 (s), 1509 (m), 1243 (s), 1216 (m), 1096 (s). UV-vis, nm in benzene, (ε, M^{-1}cm^{-1}): 480 (3796), 616 (6612), 690 (5024), 768 (3918), 912 (1018). Anal. Calc **1** + pentane. C, 67.89; H, 7.42; N, 9.21; Found: C, 68.34; H, 6.54; N, 9.98. Note: These combustion results represent the most consistent data we have obtained. Complex **2** is unstable and decomposes slowly in the solution or solid state, making obtaining accurate combustion analysis difficult.

[Fe(^{Tol,Ph}DHP)(PMe$_3$)$_2$(MeCN)][BF$_4$] (2-MeCN)

In a 20 mL vial, **1** (25 mg, 0.04 mmol, 1 eq.) was dissolved in acetonitrile (10 mL). Separately, AgBF$_4$ (7 mg, 0.04 mmol, 1 eq.) was dissolved in acetonitrile (2 mL), then added to the reaction vial dropwise with stirring to form a deep blue solution. This was allowed to stir for 20 minutes. It was then filtered and condensed under vacuum. The maroon solid was washed with toluene (5 mL), then taken up in acetonitrile, filtered, then condensed for form a concentrated solution in acetonitrile. One drop of PMe$_3$ was then added, then a vapor diffusion of diethylether into this concentrated solution of product in acetonitrile with excess PMe$_3$ was set up for final purification. Crystals could be obtained overnight at room temperature. Yield: 91% . Single crystals suitable for XRD were obtained by vapor diffusion of diethylether into acetonitrile or by vapor diffusion of petroleum ether into a solution of **2** in THF. ^{1}H NMR (400 MHz, CD$_3$CN, RT): δ = 8.12 (s, 2), 7.67 (d, 4), 2.45 (s, 6), 0.39 (bs, 16). ^{13}C{^{1}H} NMR (400 MHz, CD$_3$CN, RT): δ = 138.72, 138.22, 137.07, 135.09, 131.59, 129.61, 128.97, 127.42, 125.83, 124.78, 124.54, 20.88, 12.66. ^{31}P{^{1}H} NMR (400 MHz, CD$_3$CN, RT): δ = 6.5. ^{19}F{^{1}H} NMR (500 MHz, CD$_3$CN, RT): δ -151.9. ^{11}B{^{1}H} NMR (400 MHz, CD$_3$CN, RT): δ −1.2. IR (nujol mull, cm^{-1}): 2721 (C-H, m), 2669 (C-H, m), 2599 (C-H, w), 1957 (w), 1663 (w), 1586 (m), 1306 (s), 1283 (s), 1170 (s), 1055 (s), 933 (s). UV-vis, nm in acetonitrile, (ε, M^{-1}cm^{-1}): 534 (2661), 644 (4244), 728 (5113), 940 (1135). UV-vis, nm in acetonitrile, (ε, M^{-1}cm^{-1}): 536 (2127), 746 (2037), 676 (755). Anal. Calc. **2** + MeCN, C, 58.84; H, 5.80; N, 10.29; Found: C, 58.49; H, 5.83; N, 10.23.

[1] a) R. H. Crabtree, *Organometallic Chemistry of the Transition Metals, 6th Edition*, 2014 b).Fritz, M.; Schneider, S. In *The Periodic Table II: Catalytic, Materials, Biological and Medical Applications*; Mingos, D. M. P., Ed.; Springer International Publishing: Cham, 2019; pp 1–36.

[2] a) Liao, Q.; Liu, T.; Johnson, S. I.; Klug, C. M.; Wiedner, E. S.; Morris Bullock, R.; Dubois, D. L. *Dalt. Trans.* 2019, *48*, 4867–4878; b) K. C. Macleod, R. A. Lewis, D. E. Derosha, B. Q. Mercado and P. L. Holland, *Angew. Chem. Int. Ed.*, 2017, *56*, 1069–1072.; c) Sinha, S.; Das, S.; Sikari, R.; Parua, S.; Brandão, P.; Demeshko, S.; Meyer, F.; Paul, N. D. *Inorg. Chem.* 2017, *56*, 14084–14100.; d) Chirik, P. J. *Acc. Chem. Res.* 2015, *48* 1687–1695.; e) Liu, T.; Liao, Q.; O'Hagan, M.; Hulley, E. B.; DuBois, D. L.; Bullock, R. M. *Organometallics* 2015, *34*, 2747–2764.; f) Wong, J. L.; Sanchez, R. H.; Logan, J. G.; Zarkesh, R. A.; Zillera, J. W.; Heyduk, *Chem. Sci.* 2013, *4*, 1906–1910.; g) Kaim, W. *Inorg. Chem.* 2011, *50*, 9752–9765. h) Helm, M. L.; Stewart, M. P.; Bullock, M. R.; DuBois, M. R.; DuBois, D. L. *Science* 2011, *333*, 863–867.

[3] a) Rauch, M.; Kar, S.; Kumar, A.; Avram, L.; Shimon, L. J. W.; Milstein, D. *J. Am. Chem. Soc.* 2020, *142*, 14513–14521.; b) M. L. Pegis, C. F. Wise, D. J. Martin and J. M. Mayer, *Chem. Rev.*, 2018, *118*, 2340-2391.; c) Loewen, N. D.; Thompson, E. J.; Kagan, M.; Banales, C. L.; Myers, T. W.; Fettinger, J. C.; Berben, L. A. *Chem. Sci.* 2016, *7*, 2728–2735.; d) Hill, E. A.; Weitz, A. C.; Onderko, E.; Romero-Rivera, A.; Guo, Y.; Swart, M.; Bominaar, E. L.; Green, M. T.; Hendrich, M. P.; Lacy, D. C.; Borovik, A. S. *J. Am. Chem. Soc.* 2016, *138*, 13143–13146.; e) T. Zell and D. Milstein, *Acc. Chem. Res.*, 2015, *48*, 1979-1994.; f) M. Rakowski Dubois and D. L. Dubois, *Acc. Chem. Res.*, 2009, *42*, 1974-1982.

[4] a) Luca, O. R.; Crabtree, R. H. *Chem. Soc. Rev.* 2013, *42*, 1440–1459.; b) Chirik, P. J.; Wieghardt, K. *Science* 2010, *327*, 794–795.

[5] a) Joannou, M. V.; Hoyt, J. M.; Chirik, P. J. *J. Am. Chem. Soc.* 2020, *142*, 5314–5330.; b) R. Arevalo and P. J. Chirik, *J. Am. Chem. Soc.*, 2019, *141*, 9106-9123.; c) Gardinier, J. R.; Hewage, J. S.; Bennett, B.; Wang, D.; Lindeman, S. V. *Organometallics* 2018, *37*, 989–1000.; d) Bezdek, M. J.; Guo, S.; Chirik, P. J. *Science* 2016, *354*, 730–733.; e) E. J. Thompson and L. A. Berben, *Angew. Chem. Int. Ed.*, 2015, *54*, 11642-11646.; f) Heyduk, A. F.; Zarkesh, R. A.; Nguyen, A. I. *Inorg. Chem.* 2011, *50*, 9849–9863.

[6] a) Charette, B. J.; Ziller, J. W.; Heyduk, A. F. *Inorg. Chem.* 2021, *60*, 1579–1589.; b) T. J. Sherbow, E. J. Thompson, A. Arnold, R. I. Sayler, R. D. Britt, L. A. Berben, *Chem. - Eur. J.,* 2019, *25*, 454-458.; c) M. J. Drummond, C. L. Ford, D. L. Gray, C. V. Popescu and A. R. Fout, *J. Am. Chem. Soc.*, 2019, *141*, 6639-6650.; d) Rosenkoetter, K. E.; Wojnar, M. K.; Charette, B. J.; Ziller, J. W.; Heyduk, A. F. *Inorg. Chem.* 2018, *57*, 9728–9737.; e) M. B. Ward, A. Scheitler, M. Yu, L. Senft, A. S. Zillmann, J. D. Gorden, D. D. Schwartz, I. Ivanović-Burmazović and C. R. Goldsmith, *Nature Chem.*, 2018, *10*, 1207-1212.; f) R. Pramanick, R. Bhattacharjee, D. Sengupta, A.

Datta and S. Goswami, *Inorg. Chem.*, **2018**, *57*, 6816-6824.; g) R. Jain, A. A. Mamun, R. M. Buchanan, P. M. Kozlowski and C. A. Grapperhaus, *Inorg. Chem.*, **2018**, *57*, 13486-13493.; h) F. Schneck, M. Finger, M. Tromp and S. Schneider, *Chem. Eur. J.*, **2017**, *23*, 33-37.; i) G. W. Margulieux, M. J. Bezdek, Z. R. Turner and P. J. Chirik, *J. Am. Chem. Soc.*, **2017**, *139*, 6110-6113.; j) A. Dauth, U. Gellrich, Y. Diskin-Posner, Y. Ben-David and D. Milstein, *J. Am. Chem. Soc.*, **2017**, *139*, 2799-2807.; k) B. M. Lindley, Q. J. Bruch, P. S. White, F. Hasanayn and A. J. M. Miller, *J. Am. Chem. Soc.*, **2017**, *139*, 5305–5308.; l) P. O. Lagaditis, B. Schluschaß, S. Demeshko, C. Würtele and S. Schneider, *Inorg. Chem.*, **2016**, *55*, 4529-4536.; m) J. T. Henthorn, S. Lin and T. Agapie, *J. Am. Chem. Soc.*, **2015**, *137*, 1458-1464.; n) T. W. Myers, L. A. Berben, *Chem. Sci.*, **2014**, *5*, 2771-2777.; o) B. W. Purse, L. H. Tran, J. Piera, B. Åkermark and J. E. Bäckvall, *Chem. Eur. J.*, **2008**, *14*, 7500–7503.

[7] a) McNeece, A. J.; Jesse, K. A.; Xie, J.; Filatov, A. S.; Anderson, J. S. *J. Am. Chem. Soc.* **2020**, *142*, 10824–10832.; b) Chang, M. C.; Jesse, K. A.; Filatov, A. S.; Anderson, J. S. *Chem. Sci.* **2019**, *10*, 1360–1367.; c) Chang, M.-C.; McNeece, A. J.; Hill, E. A.; Filatov, A. S.; Anderson, J. S. *Chem. Eur. J.* **2018**, *24*, 8001–8008

[8] a) Batten, S. R.; Bjernemose, J.; Jensen, P.; Leita, B. A.; Murray, K. S.; Moubaraki, B.; Smith, J. P.; Toftlund, H. *J. Am. Chem. Soc.* **2020**, *142*, 17670−17680. b) García-Lopez, V.; Waerenborgh, J. C.; Vieira, B. J. C.; Clemente-Leon, M.; Coronado, E., *Dalton Trans.* **2018**, *47*, 9156−9163.; c) Shatruk, M.; Phan, H.; Chrisostomo, B. A.; Suleimenova, A. *Coord. Chem. Rev.* **2015**, *289−290*, 62−73.; d) Halcrow, M. A. In *Spin-Crossover Materials: Properties and Applications;* Wiley-Blackwell: Oxford, 2013.; e) Tissot, A.; Shepherd, H. J.; Toupet, L.; Collet, E.; Sainton, J.; Molnar, G.; Guionneau, P.; Boillot, M.-L. *Eur. J. Inorg. Chem.* **2013**, *2013*, 1001−1008.; f) Murray, K. S., *Eur. J. Inorg. Chem.* **2008**, *2008*, 3101−3121.

[9] a) Govor, E. V.; Al-Ameed, K.; Chakraborty, I.; Coste, C. S.; Govor, O.; Sanakis, Y.; McGrady, J. E.; Raptis, R. G. *Angew. Chem. Int. Ed.* **2017**, *56*, 582–586.; b) Min, K. S.; DiPasquale, A. G.; Rheingold, A. L.; White, H. S.; Miller, J. S. *J. Am. Chem. Soc.* **2009**, *131*, 6229–6236.

[10] a) Ravel, B., Newville, M., ATHENA, ARTEMIS, HEPHAESTUS: data analysis for X-ray absorption spectroscopy using IFEFFIT. *J. Synchr. Radn.*, **2005**, *12*, 537-541.; b) Newville, M., IFEFFIT: interactive EXAFS analysis and FEFF fitting. *J. Synchr. Radn.* **2001**, *8*, 322-324.; c) Rehr, J. J.; Albers, R. C. *Rev. Mod. Phys.* **2000**, *72*, 621-654